LBL-15458 Rev.
Preprint c.2

Lawrence Berkeley Laboratory

UNIVERSITY OF CALIFORNIA

RECEIVED
LAWRENCE
BERKELEY LABORATORY
OCT 9 1984
LIBRARY AND
DOCUMENTS SECTION

Materials & Molecular Research Division

Submitted to Journal of the Electrochemical Society

NUCLEATION OF Pb ELECTRODEPOSITS ON Ag AND Cu

J.C. Farmer and R.H. Muller

August 1984

TWO-WEEK LOAN COPY
This is a Library Circulating Copy
which may be borrowed for two weeks.

Prepared for the U.S. Department of Energy under Contract DE-AC03-76SF00098

LBL-15458 Rev. c.2

DISCLAIMER

This document was prepared as an account of work sponsored by the United States Government. While this document is believed to contain correct information, neither the United States Government nor any agency thereof, nor the Regents of the University of California, nor any of their employees, makes any warranty, express or implied, or assumes any legal responsibility for the accuracy, completeness, or usefulness of any information, apparatus, product, or process disclosed, or represents that its use would not infringe privately owned rights. Reference herein to any specific commercial product, process, or service by its trade name, trademark, manufacturer, or otherwise, does not necessarily constitute or imply its endorsement, recommendation, or favoring by the United States Government or any agency thereof, or the Regents of the University of California. The views and opinions of authors expressed herein do not necessarily state or reflect those of the United States Government or any agency thereof or the Regents of the University of California.

LBL-15458 - Rev.

NUCLEATION OF Pb ELECTRODEPOSITS ON Ag AND Cu

Joseph C. Farmer and Rolf H. Muller

Lawrence Berkeley Laboratory
University of California
Berkeley, California 94720

August 1984

This work was supported by the Director, Office of Energy Research, Office of Basic Energy Sciences, Materials Sciences Division of the U.S. Department of Energy under Contract No. DE-AC03-76SF00098.

LBL-15458 - Rev.

NUCLEATION OF Pb ELECTRODEPOSITS ON Ag AND Cu

Joseph C. Farmer and Rolf H. Muller

Materials and Molecular Research Division
Lawrence Berkeley Laboratory &
Department of Chemical Engineering
University of California, Berkeley 94720

ABSTRACT

Initial stages in the electrocrystallization of Pb (up to 200 Å thickness) from 1 M $NaClO_4$, 0.5 and 5 mM Pb $(NO_3)_2$, pH 3, on Ag(111) and Cu(111) have been investigated by ellipsometry and light scattering during cyclic voltammetry. Optical constants, thickness, valence, and free energy of adsorption of the underpotential deposit have been determined. An optical model which agrees with experimental data for fractional coverage by the underpotential deposit is based on the two-dimensional spreading of islands of monolayer thickness. The bulk deposit immediately following formation of the underpotential monolayer involves three-dimensional growth from nucleation centers, even at the 20 Å level of deposit thickness, and results in a particulate, porous film on top of the underpotential deposit.

Keywords: Metals, Surfaces, Ellipsometry, Light scattering, Chemisorption.

Introduction

Two separate steps can often be identified in the early stages of the electrocrystallization of a metal on a dissimilar substrate, the formation of an underpotential deposit (UPD) and a bulk deposit (1-3). The properties of these layers are expected to be an inportant factor for determining the properties of subsequently formed deposits of practical interest with macroscopic thicknesses. This work was undertaken to investigate the transition from the underpotential deposit (the first monolayer) to the bulk deposit and the micromorphology of the two deposits by *in situ* optical techniques. Fast automatic ellipsometry and light scattering during cyclic voltammetry made it possible to separate optical changes due to formation of the first monolayer from those associated with subsequent formation of the bulk deposit. The system chosen for study was the deposition of Pb on Ag and Cu because of the well-known formation the underpotential layers (4). There are also significant differences in the optical constants of Pb and the substrates, making detection of small amounts of Pb on the electrode surface by ellipsometry possible (5-7).

Schmidt and Gygax (3) have determined the Gibbs free energy of adsorption for Pb electrosorption on polycrystalline Ag and Cu by integrating the cathodic UPD peak in the cyclic voltammogram and deriving coverage as a function of potential. Here, adsorption isotherms for the Pb underpotential deposit have been determined similarly on single crystal Ag and Cu surfaces. In addition, thickness and optical constants of the underpotential deposit were derived from ellipsometer measurements and a knowledge of surface coverage determined electrochemically. Unusual optical properties of the bulk deposit have been attributed to its morphology.

Experimental Procedure

Experiments were conducted potentiodynamically while simultaneous ellipsometer and light scattering measurements of the electrode surface were performed. A bipotentiostat (Pine RDE 3) was used to drive the electrochemical cell. The potential was swept from 200 to -800 mV (vs. Ag/AgCl) at sweep rates varying from 0.1 to 1.5 volts per minute.

A self-nulling ellipsometer (8) was operated at an angle of incidence of 75 deg. with a stabilized 75 W Xenon short-arc light source (Oriel C-72-20) and an interference filter for 515 nm (bandwidth 9 nm, transmission 43%). An acrylic electrolytic cell used in an earlier investigation of anodic silver oxidation (9) was employed. The cell had two quartz windows for ellipsometry with an angle of incidence of 75 degrees, a volume of approximately 250 ml and ports for introduction and draining of electrolyte, for a nitrogen purge stream, and for a reference electrode capillary. A Pt counter electrode was used and positioned so as not to interfere with the observation of the working electrode.

Ag(111) and Cu(111) working electrodes were used. The single-crystal surfaces were approximately 1.20 cm x 2.85 cm (3.42 cm^2), and were mounted in epoxy. The electrodes were polished mechanically, ultimately using 0.05μm aluminum oxide powder suspended in water. The polishing was followed by ultrasonic cleaning, chemical polishing for Ag surfaces (9,10) a period of soaking in the acidic electrolyte, and pre-electrolysis. Any oxides formed on the electrode surface during transfer to the cell were unstable at the pH and potential used for the experiments and removed during pre-electrolysis at a potential anodic to that for Pb deposition (11,12). No significant electrochemical or ellipsometric differences were

observed between Ag electrodes polished mechanically and chemically and those polished only mechanically, although a smoother surface important for light scattering measurements was expected to result from chemical polishing. The chemical polishing step was omitted after scattering measurements were completed.

The reference electrode used was a double-junction Ag/AgCl electrode (Dow-Corning 476067). The inner compartment containing the electrode, was filled with 4 M KCl saturated with AgCl, the outer compartment with 1 M KNO_3.

A second cell was used for light scattering studies, and has been described elsewhere (9). This cell used high-purity, polycrystalline Ag sheets rather than single crystals. The electrode was 0.5 cm x 5.0 cm x 0.2 cm and was 60% immersed in electrolyte. It was located in a cylindrical glass cell of 4 cm diameter and illuminated with the beam from an argon laser (515 nm line) at an angle of incidence of 75 degrees.

All experiments used a supporting electrolyte of 1 M $NaClO_4$ at pH 3. Pb^{++} ion was introduced into the electrolyte as a nitrate at concentrations of either 0.5 or 5.0 mM. The pH was adjusted to the desired level by adding small amounts of dilute $HClO_4$, and measured with a digital pH meter (Corning 130).

Experimental Results

Potential ramp and cyclic voltammogram data for the deposition of Pb on Ag(111) from a 0.5 mM solution at a sweep rate of 0.1 V/min are shown in Figs. 1 and 2.

Ellipsometer measurements (psi and delta) during two potential cycles for deposition on silver are shown in Figs. 3 and 4 together with the current trace. The separate formation of underpotential and bulk deposits is clearly shown by the relative amplitude parameter psi (Fig. 3). During the anodic part of the potential cycle the two layers are dissolved in reverse order and the process is repeated in the next cycle. Reversibility and reproducibility are also seen in the relative phase parameter delta (Fig. 4). The response of that measurement to the underpotential deposit is representative of a metal-like layer while dielectric-like properties are indicated for the bulk deposit. These unexpected optical results for delta are caused by the micromorphology of the deposits: the cathodic UPD peaks have been interpreted as the formation of a complete monolayer of Pb on the substrate; the bulk deposit is shown to be of a particulate, porous nature. Similar results were obtained for potentiodynamic deposition of Pb on Cu(111) at concentrations of 0.5 and 5.0 mM and a sweep rate of 1.5 V/min.

Light scattering measurements from the electrode surface during cyclic voltammetry are shown in Fig. 5 An argon-ion laser (Lexel 75.2) tuned to 514.5 nm, served as light source (30 mW, 75° angle of incidence). Scattered light was collected 15 degrees from the specular direction with a fiber-optic probe (1 deg. acceptance) and measured with a photomultiplier (RCA R136). The lower oscillogram traces in Fig. 5 represent the current passed through the cell, with cathodic peaks shown negative, anodic peaks positive. The poor cathodic peak waveform is due to the electrode geometry in the scattering cell, which results in non-uniform current distribution. The upper traces represent the photomultiplier current. Figure 5b shows the increase in scattered light intensity with the onset of bulk deposition and its return to the initial level upon

stripping the deposit. A particle diameter of 16 Å, derived from ellipsometer measurements, has been associated with a significant increase in light scattering. No increase in scattering light intensity is observed during formation of the underpotential deposit layer. Light scattering, like the ellipsometer measurements, are reversible and repeatable during potential cycling. Increased light scattering is indicative of the formation of very small three-dimensional nuclei appearing on top of the Pb monolayer which completely covers the substrate. This interpretation agrees with that found for the ellipsometer measurements.

Optical Model of the Initial Stage of Deposit Formation

The general theory for sub-monolayer ellipsometry has been reviewed by Bootsma (13,14). Other authors who have written on this topic have paid particular attention to the anisotropic nature of the adsorbate layer (15-17).

As discussed eleswhere (18) it has been found that the ellipsometer measurements of the formation of the underpotential deposit can best be interpreted with a coherent superposition (island) model; the Bruggeman model failed to explain the data. In this model it is assumed that the surface is partially bare and partially covered with patches or islands of a thin film (19). With the islands having a smaller diameter than the spacial coherence of the incident light, the state of polarization of the reflected light is determined by the coherent superposition of polarization states resulting from reflection on bare and film-covered surface elements.

Application of this island concept to the underpotential deposit implies that (1) metal adatoms adsorbed to the surface, as two-dimensional clusters or individually, can be treated as equivalent thin-film islands of some apparent thickness and complex refractive index; (2) the optical

constants and thickness of individual islands are the same as those of the complete monolayer; (3) the overall reflectance of the surface is due to a coherent superposition of beams reflected from island-covered portions of the electrode and bare portions of the electrode; and (4) the optical constants of the individual islands and the substrate are potential and coverage independent. Predictions derived from this model agree well with experimental data for the development of the underpotential deposit monolayer as the potential is ramped (Fig. 6). Assumption (1) above requires elaboration. As will be shown in the discussion that follows, the Pb UPD obeys a Langmuirian adsorption isotherm, which indicates that there is minimal lateral interaction between adsorbed Pb atoms, while clustering would require strong attraction. Based upon the isotherm alone, one would expect the Bruggeman optical model for a layer of randomly distributed atoms to fit the data. This dilemma will have to be resolved by future work.

An investigation of different optical models to interpret the present in situ ellipsometer measurements of the bulk deposit has been reported elsewhere (20). This layer was found to form on top of the first monolayer of Pb adatoms and to be of a granular, porous form. The optical properties of this layer are intermediate between those of metallic Pb and electrolyte and have been determined by use of the Bruggeman theory (21). This approach is analagous to that used by representing microrough surfaces as equivalent films (21-23).

Other investigators have suggested that three-dimensional nucleation occurs on a completely formed monolayer, on the basis of ex situ experiments using Auger spectroscopy (24), x-ray fluorescence (25), and scanning electron microscopy (26).

To model both the UPD monolayer and the bulk deposit collectively, a two-film model is used, analagous to the approach of Smith and Muller (19,27). First, one calculates a value of the complex reflection coefficient ratio due to the UPD layer on the electrode. Then, using this ratio, an apparent refractive index is calculated, which includes both the effects of the substrate and the UPD monolayer. The optical effect (delta and psi) of the porous bulk deposit is then determined on the apparent substrate. The Bruggeman theory is used to compute the effective refractive index of the porous film material.

By minimizing the sum-of-squares error between the model predictions and the measurement of delta and psi, one determines optimum values of the adjustable model parameters (28,29). Parameters to be fitted are (1) complex refractive index of the UPD, (2) apparent thickness of the UPD, (3) porosity of the bulk deposit, and (4) thickness of the bulk deposit. Fine tuning of the metal optical constants is done initially to compensate for uncertainty in the optical constants found in the literature or determined experimentally. Equation 1 defines the sum-of-squares error for the model.

$$S_{\Delta,\psi} = \sum_{i=1}^{N} (\Delta_{M,i} - \Delta_{C,i})^2 + \sum_{i=1}^{N} (\Psi_{M,i} - \Psi_{C,i})^2 \qquad (1)$$

The parameter variance is then defined by

$$SE(p) = \frac{\sigma^2}{\frac{1}{2}\frac{\partial^2 S_{\Delta,\psi}}{\partial p^2}} \qquad (2)$$

Parameter confidence intervals (Eq. 3) are calculated from this variance and the student-t statistic for 2N-P degrees of freedom, where N is the number of delta-psi measurements and P is the number of adjustable model parameters.

$$\delta(p) = t(2N - P, 1 - 2\alpha)[SE(p)]^{1/2} \tag{3}$$

Both the parameter variance and the model variance are required, and are estimated numerically by use of Eqs. 4 and 5, respectively.

$$\sigma^2 \sim S_{MIN}/df = S_{MIN}/(2N - P) \tag{4}$$

$$\frac{1}{2}\frac{\partial^2 S_{\Delta,\psi}}{\partial p^2} \sim \frac{S_{(+)} + S_{(-)} - 2\,S_{MIN}}{2(\Delta p)^2} \tag{5}$$

Separate optimizations are performed to determine UPD and bulk optical properties. This is possible since potential ramping separates formation of the two layers in time. As the UPD was formed, 19 values of current, delta, and psi were logged by computer during formation of the Pb UPD on Ag; these measurements were used collectively to determine the three parameters needed for the characterization of the UPD (complex refractive index and thickness). These values can be determined from data for a single cathodic sweep with a high degree of accuracy. Optical constants and thicknesses determined thus for the Pb UPD layer on Ag(111) and Cu(111) for a wavelength of 515 nm are given in Table I (18) The error limits are given for a 95% level of confidence, based upon 37 degrees of freedom. The thickness of the layer of 4-5 Å compares well with an atomic diameter of about 3.5 Å.

Estimates of the parameters for the bulk deposit are more uncertain. Confidence intervals for these parameters can only be derived by averaging comparable values of delta and psi from replicate experiments (or multiple sweeps). Modeling results for the bulk Pb deposit are presented in Table II for different substrates, electrolytes and potential cycles. From these results it was concluded that the bulk deposit formed in the experiments conducted with 0.5 mM was approximately 30% porous and about 10 Å thick; the bulk deposit formed with 5.0 mM was approximately 40% porous and 200 Å thick.

Adsorption Isotherm

Conway, Kozlowska, and Dahr present general theories of adsorption at liquid-solid interfaces and the proper selection of standard states (30). Conway and Kozlowska also discuss the effects of sweep rate, etc. on the UPD peak in voltammetry (31). Ross has shown that the Langmuir isotherm can be applied to hydrogen adsorption on Pt single crystals with data taken from cyclic voltammograms (32). Swathirajan, Mizota, and Bruckenstein have presented a detailed thermodynamic model for Ag and Pb underpotential deposition on polycrystalline Au, and determined that both of these UPD layers involved electrosorbed species having valences equivalent to those of their respective dissolved ions (33). If one assumed that the valence of the electrosorbed Pb species on Ag(111) and Cu(111) is equivalent to that of Pb^{2+}, the term $RT/F(1/\gamma_{UPD} - 1/z) \ln a_{M^{2+}}$ in Eqn. 12 of Ref. 33 becomes zero, and the adsorption behavior is therefore independent of the solution activity of Pb^{2+}. The terms γ_{UPD}, z and $a_{M^{2+}}$ correspond to the terms z, z_{Pb} and a, respectively in this paper. By assuming that both the Frumkin and Temkin parameters are zero, and by taking the reference potential $U_{1/2}$,

to be that giving $\theta = 0.5$, Eqn. 12 of Ref. 33 reduces to the Langmuir isotherm, Eqn. 6, which is linear in potential

$$\ln\left(\frac{\theta}{1-\theta}\right) = -\frac{zF}{RT}(U-U_{1/2}) \tag{6}$$

The Gibbs free energy of adsorption is related to the underpotential at half monolayer coverage ($U_{1/2}$) through Eq. 7.

$$\Delta G^{\circ}_{ADS} = -zFU_{1/2} \tag{7}$$

Since Eq. 6 is linear in potential (underpotential scale), it can be applied to experimental data easily by using regression analysis (34). Eq. 8 is used for data reduction; the slope m and intercept b are then related to the Gibbs free energy of adsorption.

$$\ln\left(\frac{\theta}{1-\theta}\right) = m \cdot U + b \tag{8}$$

$$G^{\circ}_{ADS} = -bRT \tag{9}$$

The underpotential at half-coverage and the apparent valence are given by Eqs. 10 and 11, respectively.

$$U_{1/2} = -b/m \tag{10}$$

$$z = -m\,RT/F \tag{11}$$

Rigorous analysis relates the error in these physical quantities (Eqns. 12 through 14) to the uncertainties in the slope and intercept of the regression line (Eqns. 15 and 16), and to the model variance (Eq. 17).

$$\delta(\Delta G^{\circ}_{ADS}) = F\left[(U_{1/2}\cdot\delta z)^2 + (z\cdot\delta U_{1/2})^2\right]^{1/2} \tag{12}$$

$$\delta(U_{1/2}) = U_{1/2}\left[\left(\frac{\delta b}{b}\right)^2 + \left(\frac{\delta m}{m}\right)^2\right]^{1/2} \tag{13}$$

$$\delta(z) = \frac{RT}{F}\,|\delta m| \qquad \text{(also written as } \delta z\text{)} \tag{14}$$

$$\delta m = S\cdot t(N-2,\ 1-2\alpha)\left[\sum_{i=1}^{N}(U_i-\overline{U})^2\right]^{-1/2} \tag{15}$$

$$\delta b = S\cdot t(N-2,\ 1-2\alpha)\left[\left(\sum_{i=1}^{N}U_i^2\right)\div\left(N\sum_{i=1}^{N}(U_i-\overline{U})^2\right)\right]^{1/2} \tag{16}$$

$$S = \left[\sum_{i=1}^{N}\left(\ln\left(\frac{\theta_i}{1-\theta_i}\right) - \ln\left(\frac{\theta_u}{1-\theta_u}\right)\right)^2 \frac{1}{N-2}\right]^{1/2} \tag{17}$$

Results of the linear regression and error analysis are presented in Table III. The data for the Pb UPD on Ag(111) and Cu(111) were first analyzed separately; then together. The non-integer values of the electrosorption valence could imply that Frumkin and Temkin parameters should be included in the adsorption isotherm model; however, it is believed that these unusual values are attributable to integration errors at low coverage and have no physical significance. The coverage, which is determined by

integration of the cathodic UPD peak, cannot be determined accurately at low values since the current is of the same order as the background noise.

Inspection of the experimental data plotted in Fig. 7 shows that the underpotential at half-coverage is about 155 mV for both substrates, which corresponds to a Gibbs free energy of adsorption of 7.14 kcal/mol for an assumed electrosorption valence of $z = 2$ (35). Note that a value of 5 kcal/mol has been reported for polycrystalline substrates (3). Theoretical predictions of coverage at different potentials can be made by substituding these values into the adsorption isotherm equation. These predictions are represented by the broken line in Fig. 7, which agrees well with experimental data except at very low coverages. Continuous adsorption isotherms have been reported for different Ag faces (36).

Double layer charging currents were subtracted by base-line extrapolation across the base of the UPD peak, assuming the a priori separability of charging currents. This method can lead to errors in coverage estimation, but the error for the Pb UPD on Ag and Cu may be small if the points of zero charge (PZC's) of the two materials are nearly equal (37). The concept of partial discharge associated with electrosorption bonds (38) in the underpotential deposit is not supported by this work.

Charge Balance

Equation 18 was used to calculate the charge passed to the working electrode during deposition.

$$Q = \int_0^t i\,(t)\cdot A\cdot dt = \frac{(x\cdot y\cdot d_q)\rho_{Pb}}{MW_{Pb}}\; z_{Pb} e\, N_{AVG} \qquad (18)$$

This charge was used to calculate the coverage of Pb adatoms on the electrode surface. The actual charge required for a complete UPD agreed with that expected for a monolayer with a roughness factor of 1.25.

The thickness of the bulk deposit and the volume fraction of Pb in it, determined from ellipsometer measurements, were used to compute the total amount of Pb on the electrode surface. This quantity was then compared to the amount expected on the basis of charge passed. The ellipsometer measurements consistently predict less Pb on the surface than the charge balance (a discrepancy ranging from 10 to 50 percent, Table IV). This difference might be due to uneven current distribution on the electrode, with more Pb being deposited around the edge of the electrode, while the ellipsometer measurement was performed at the center.

Conclusions

The initial stages of electrodeposition (0 to 200 Å) can be elucidated by the simultaneous use of ellipsometry, cyclic voltammetry, and light scattering measurements. The application of a potential ramp allows one to separate underpotential and bulk deposits in time and thus investigate them separately.

An optical model which fits the data very well involves the two-dimensional growth of monolayer islands during UPD formation and the three-dimensional nucleation and growth of a microporous bulk deposit on top of it. Thickness, optical constants, Gibbs free energy of adsorption and apparent valence for the Pb UPD on Ag(111) and Cu(111) have been determined.

Acknowledgments

This work was supported by the Director, Office of Energy Research, Office of Basic Energy Sciences, Materials Sciences Division of the U.S. Department of Energy under contract no. DE-AC-03-76SF00098. We wish to thank W.J. Plieth for use of the light-scattering cell.

This was paper 823 presented at the San Francisco, California meeting of the Society, May 8-13, 1983.

NOMENCLATURE

$\hat{A}$	electrode area (cm^2)
$\hat{A}$, $\hat{B}$	complex parameters for quadratic equation
a	activity of Pb^{2+} in solution
b	linear regression intercept
C	concentration
d	thickness of bulk deposit derived from ellipsometer measurement
d_{UPD}	thickness of underpotential deposit
df	degrees of freedom, 2N-P
d_q	deposit thickness based on change (Å)
e	electronic charge (1.602×10^{-19} C)
E	electrode potential vs. Ag/AgCl (V)
F	Faraday constant (96487 Coul/equiv.)
g	interaction parameter
i(t)	time-varying current density during cyclic voltammetry (A/cm^2)
k_{UPD}	extinction coefficient of underpotential deposit
k_{Pb}	extinction coefficient of bulk Pb
m	slope of linear regression (V^{-1})
MW_{Pb}	atomic weight of Pb(207.2g/mol)
n_{Pb}	refractive index of bulk Pb

n_{UPD}	refractive index of underpotential deposit
N	number of data points defining experimental electrosorption isotherm and number of pairs of Δ and ψ measurements
N_{AVG}	Avagadro's number (6.02×10^{23} at/mol)
N_i	atomic number density of component i in the effective medium
p	arbitrary model parameter to be fitted
P	number of model parameters to be fitted
Q	total charge passed to working electrode (C)
r	regression coefficient (Table III)
RT	constant (0.592 kcal/mol)
S	variance between experimental data and prediction of electrosorption model
S( )	error of quantity in parentheses (except for $\delta\Delta$ and $\delta\psi$)
SE(p)	variance of parameter p
$S_{\Delta,\psi}$	sum-of-squares error between theoretical ellipsometer parameters and those measured experimentally
S_{MIN}	minimum value of $S_{\Delta,\psi}$ corresponding to a selection of optimum "p" values

$S_{(+)}$	value of $S_{\Delta,\psi}$ computed at a parameter value of $p + \Delta p$
$S_{(-)}$	value of $S_{\Delta,\psi}$ computed at a parameter value of $p - \Delta p$
t	time
$t(2N-P,\ 1-2\alpha)$	the t-statistic for "2N-P" degrees-of -freedom at a "1-2α" level of confidence
U	underpotential relative to Nernst potential E°(V)
U_i	measured value of U (controlled) at the i-th coverage; the i-th data point
$U_{1/2}$	underpotential corresponding to $\theta = 0.5$(V)
$\overline{U}$	mean underpotential (V)
V	electrode potential (V)
x	electrode dimension (cm)
y	electrode dimension (cm)
z	apparent valence of metal adatom after electrosorption
z_{Pb}	valence of lead ion in solution (2)

α	level of confidence, $1-2\alpha$
$\delta(p)$	error in parameter "p" at a "$1-2\alpha$" level of confidence
$\delta\Delta$	change in ellipsometer parameter delta due to underpotential deposit (deg)
$\delta\psi$	change in ellipsometer parameter psi due to underpotential deposit (deg)
Δ or delta	ellipsometer parameter, phase difference between p and s electric field components after reflection, relative to the incident (degrees)
Δ_C	calculated value of Δ for bulk deposit
$\Delta_{C,i}$	calculated value of Δ corresponding to $\Delta_{M,i}$
Δ_M	measured value of delta for bulk deposit (deg)
$\Delta_{M,i}$	the i-th measured value of Δ for the UPD at the i-th coverage; the i-th data point
ΔG°_{ADS}	Gibbs free energy of adsorption for UPD monolayer (kcal/mol)
θ	fractional coverage of electrode surface by UPD monolayer
θ_f	fraction of surface covered by film of refractive index $\hat{n}_f$
θ_i	UPD monolayer coverage measured at underpotential U_i
θ_{Pb}	volume fraction of Pb in composite thin -film deposit

θ_u	monolayer coverage predicted by electrosorption model for underpotential U_i
ρ_{Pb}	density of Pb (11.34 g/cm^3)
σ^2	variance of the model predictions for Δ and ψ
ψ or psi	ellipsometer parameter, amplitude ratio of p and s electric field components after reflection (tan ψ), relative to the incident (degrees)
ψ_C	calculated value of ψ for bulk deposit
$\psi_{C,i}$	calculated value of ψ corresponding to $\psi_{M,i}$
$\psi_{M,i}$	measured value of ψ for the UPD at the i-th coverage; the i-th data point
ψ_M	measured value of psi for bulk deposit (deg)

References

1. D. M. Kolb, in Advances in Electrochemistry and Electrochemical Engineering, Vol. 11, edited by H. Gerischer and C. W. Tobias, Wiley, New York, 1978, pp. 125-271.

2 J. A. Harrison and H. R. Thirsk, in Electroanalytical Chemistry, Vol. 5, edited by A. J. Bard, Dekker, New York (1971).

3. E. Schmidt and H. R. Gygax, J. Electroanal. Chem., 12, 300 (1966).

4. K. Jüttner and W. J. Lorenz, Z. Phys. Chem. N.F. 122, 163 (1980).

5. G. Hass and L. Hadley, in American Institute of Physics Handbook, 2nd ed., edited by D. E. Gray, McGraw-Hill, New York, (1963).

6. P. B. Johnson and R. W. Christy, Phys. Rev. B, 6, 4370 (1972).

7. R. Adzic, E. Yeager and B. D. Cahan, J. Electrochem. Soc., 121, 474 (1974).

8. H. J. Mathieu, D. E. McClure and R. H. Muller, Rev. Sci. Instrum., 45, 798 (1974).

9. R. H. Muller, W. J. Plieth and J. C. Farmer, Lawrence Berkeley Laboratory, LBL-12965 (1981).

10. G. Petzow, Metallographisches Atzen, Borntraeger, Berlin, English translation by ASM (1976).

11. P. Delahay, M. Pourbaix and P. Van Rysselberghe, J. Electrochem. Soc., 98, 65 (1951).

12. M. Pourbaix, Atlas of Electrochemical Equilibria in Aqueous Solutions, Pergamon, New York (1966).

13. G. A. Bootsma and F. Meyer, Surf. Sci. 14, 52 (1969).

14. G. A. Bootsma, L. J. Hanekamp and O.L.J. Gijzeman, Proceedings 5th Summer Institute for Surface Science, edited by R. Howe, R. Vanselow, Springer, Berlin (1982).

15. A. M. Brodski and M. I. Urbakh, Sov. Electrochem., 38, 1553 (1979).

16. W. Plieth, H. Bruckner and H.-J. Hensel, Surf. Sci., 101, 261 (1980).

17. K. Takamura, F. Watanabe and T. Takamura, Electrochim. Acta, 26, 979 (1981).

18. R. H. Muller and J. C. Farmer, Surf. Sci., 135, 521 (1983).

19. R. H. Muller and C. G. Smith, Surf. Sci., 96, 375 (1980).

20. R. H. Muller and J. C. Farmer, Proc. Intl. Conf. on Ellipsometry and other Optical Methods for Surface and Thin Film Analysis, Paris, 7-10 June 1983, J. Phys. 44, C10-57 (1983).

21. D. E. Aspnes, J.B. Theeten and F. Hottier, Phys. Rev., B, 20, 3292 (1979).

22. K. Brudzewski, Thin Solid Films, 61, 183 (1979).

23. T. Smith, P. Smith and F. Mansfeld, J. Electrochem. Soc., 126, 799 (1979).

24. K. Takayanagi, D. M. Kolb, K. Kambe and G. Lehmpfuhl, Surf. Sci., 100, 407 (1982).

25. B. H. Vassos and H. B. Mark, Jr., J. Electroanal. Chem., 13, 1 (1967).

26. V. V. Povetkin and I. M. Kovenskii, Sov. Electrochem., 17, 1461 (1981).

27. C. G. Smith, Ph.D. Thesis, Dept. of Chem. Engr., University of California, Berkeley, LBL-8082 (1978).

28. C. Hendrix, "An R/D Tehnical Education Course in Recent Advances in Statistics, Lecture No. 2," Union Carbide Technical Center, So. Chas., WV, April 18, 1978.

29. G.E.P. Box and G. A. Coutie, Proc. Inst. Electr. Engrs., 102, Part B, Suppl. 1, 100 (1956).

30. B. E. Conway, H. Angerstein-Kozlowska and H. P. Dhar, Electrochim. Acta, 19, 455 (1974).

31. B. E. Conway and H. Angerstein-Kozlowska, J. Electroanal. Chem., 113, 63 (1980).

32. P. N. Ross, Jr., Proc. 5th Int. Summer Institute for Surface Sciences, edited by R. Howe and R. Vanselow, Springer, Berlin (1982).

33. S. Swathirajan, H. Mizota and S. Bruckenstein, J. Phys. Chem., 86, 2480 (1982).

34. W. J. Dixon and F. J. Massey, Jr., Introduction to Statistical Analysis, McGraw-Hill, New York (1969).

35. H. Bort, K. Jüttner and W. T. Lorenz, J. Electroanal. Chem., 90, 413 (1978).

36. W. J. Lorenz, E. Schmidt, G. Staikov and H. Bort, Farraday Disc. Chem. Soc. No. 12, Farraday Symp. 12, 14 (1978).

37. S. Swathirajan and S. Bruckenstein, J. Electroanal. Chem., 146, 137 (1983).

38. E. E. Mola, Electrochim. Acta, 26, 1253 (1983).

Table I. Optical Properties of the Pb Underpotential Deposit (UPD) at Complete Coverage (θ=1). Wavelength, 514.5 nm; electrolyte, 0.5 and 5.0 mM Pb^{++} 1 M $NaClO_4$, pH 3; errors given for 95% level of confidence.

Substrates		Ag(111)	Cu(111)	Cu(111)
Pb concentration (mM)		0.5	0.5	5
UPD refractive index	n_{UPD}	1.285±0.007	1.225±0.066	0.952±0.417
UPD extinction coeff.	k_{UPD}	4.080±0.040	3.520±0.041	3.898±0.021
UPD thickness (Å)	d_{UPD}	5.149±0.026	4.030±0.178	4.777±1.101

Table II. Optical Properties of Bulk Pb Deposits from 1 M $NaClO_4$ Supporting Electrolyte at pH 3, Electrode Area 3.42 cm^2, Underpotential Deposit indicated by *.

t(sec)	E (mV)	Q(mC)	d_q(Å)	Δ_M	ψ_M	Δ_C	ψ_C	d(Å)	θ_{Pb}	n_{Pb}	k_{Pb}
					Ag(111), 0.5 mM Pb^{++}, 0.1 V/min						
219*	-443	1.55	3.52	72.06	43.27	72.06	43.27	5.53	1	1.30	4.27
300	-490	12.93	29	71.90	41.85	71.58	41.97	16	0.75	2.05	4.27
413	-663	18.35	42	71.62	41.13	71.30	41.18	26	0.75	2.10	4.27
					Cu(111), 0.5 mM Pb^{++}, 0.5 V/min						
18*	-452	1.58	3.52	60.31	38.44	60.32	38.43	5.05	1	1.35	4.03
24	-592	2.20	5	60.56	38.22	60.52	38.13	6	0.71	1.95	4.27
30	-746	3.14	7	60.61	38.11	60.61	38.11	6	0.71	1.95	4.27
46	-476			60.61	37.90	60.51	38.14	6	0.71	1.95	4.27
48	-438	4.47	10	60.83	37.84	60.82	37.80	12	0.73	1.98	4.24
					Cu(111), 5.0 mM Pb^{++}, 1.5 V/min						
17*	-422	2	3.52	59.34	38.04	59.32	37.97	4.79	1	0.95	3.99
23	-576	28	49	56.59	36.17	56.52	36.09	76	0.56	1.90	4.30
40	-606	80	141	58.00	33.95	58.01	34.03	170	0.60	1.94	4.26
45	-478	91	160	58.55	33.56	58.63	33.16	194	0.61	1.99	4.28

Table III. Linear Regression Analysis of Adsorption Isotherm Data.

QUANTITY	UNITS	Ag(111)	Cu(111)	Ag(111)+Cu(111)
ΔG°_{ADS}	kcal/mol	-8.75	-7.75	-7.90
$U_{1/2}$	mV	151	156	155
z		2.52	2.15	2.21
m	mV^{-1}	-0.098.26	-0.083678	-0.086188
b		14.783091	13.090754	13.339047
$\delta(\Delta G^{\circ}_{ADS})$	kcal/mol	1.23	0.87	0.88
$\delta(U_{1/2})$	mV	17	13	15
$\delta(z)$		0.21	0.12	0.12
$\delta(m)$	mV^{-1}	0.008001	0.004746	0.004523
$\delta(b)$		1.134927	0.800944	0.706471
S		0.485484	0.437346	0.572739
r		-0.989448	-0.992104	-0.986668

Note: $N-2 = 17$, $1-\frac{\alpha}{2} = 0.95$, and $t(17, 0.95) \sim 2.11$

$N-2 = 36$, $1-\frac{\alpha}{2} = 0.95$, and $t(36,0.95) \sim 2.02$

Table IV. Comparison of Amount of Pb Deposit d_q Based on Charge Passed with Amount $\theta_{Pb}.d$ Derived from Ellipsometer Measurement.

SUBSTRATE	Pb^{++} mM	time sec	d_q Å	θ_{Pb} vol. fract.	d Å	$\frac{\theta_{Pb}.d}{d_q}$
Ag(111)	0.5	300	29	0.75	16	0.41
		413	42	0.75	26	0.46
Cu(111)	0.5	24	5	0.71	6	0.85
		30	7	0.71	6	0.61
		46	9	0.71	6	0.47
		48	10	0.73	12	0.88
Cu(111)	5.0	23	49	0.56	76	0.87
		40	141	0.60	170	0.72
		45	160	0.61	194	0.74

Figure Captions

1. Cyclic voltammogram for Pb deposition on Ag(111) (3.42 cm^2) from 1 M $NaClO_4$, 0.5 mM $Pb(NO_3)_2$, pH 3, first sweep. Potential relative to Ag/AgCl reference. Pt counter electrode, acrylic cell.
2. Potential ramp corresponding to Fig. 1 from +150 mV to -660 mV, sweep rate 0.15 V/min.
3. Response of current and ellipsometer parameter psi to potential ramp shown in Fig. 2. Wavelength of light 515 nm, angle of incidence 75 deg., other conditions as in Fig. 1.
4. Response of current and ellipsometer parameter delta, conditions as in Fig. 3.
5. Light scattering data at conditions similar to those of Fig. 1, except that the experiments were conducted on polycrystalline Ag in a light scattering cell. Top traces, scattered light intensity (increasing in the positive direction); bottom traces, current response to the potential ramp (cathodic peaks negative). The first cathodic peak, UPD deposition, the second, bulk deposition. Light source argon ion laser at 515 nm. (a) increase of light scattering with onset of bulk deposition, (b) stability of deposit on open circuit, (c) removal of deposit after open circuit stand.
6. Prediction by optimized coherent superposition model (solid line) and measurement of changes in ellipsometer parameters psi and delta due to progressive deposition of an underpotential layer of Pb on Ag(111). Properties of the underpotential deposit derived from this optimized data fit given in Table I.

7. Electrosorption isotherm for Pb UPD on Ag(111) and Cu(111), model predictions for a free energy of adsorption of 7 kcal/mol and a valence of 2 (broken line) and experimental data from cyclic voltammetry. Coverage computed from charge.

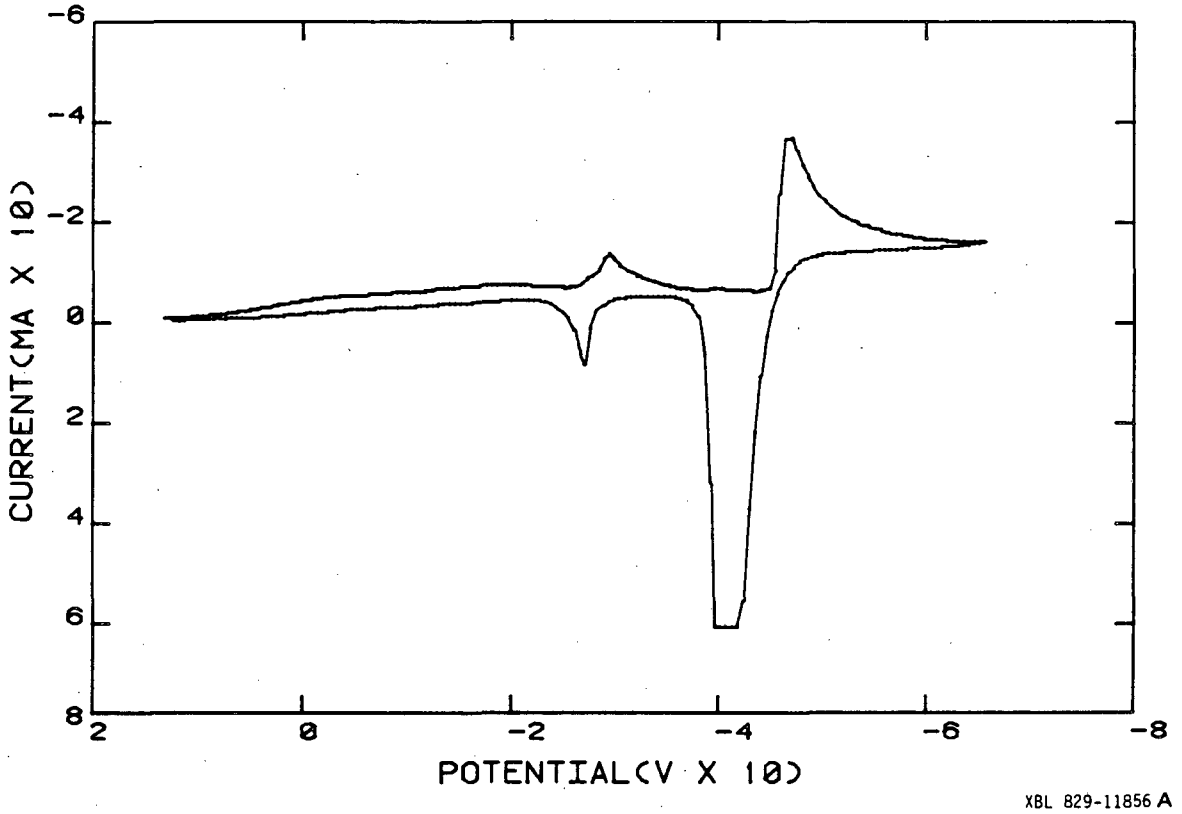
-6
-4
-2
0
2
4
6
8
CURRENT(MA X 10)
2
0
-2
-4
-6
-8
POTENTIAL(V X 10)
XBL 829-11856 A

Fig. 1

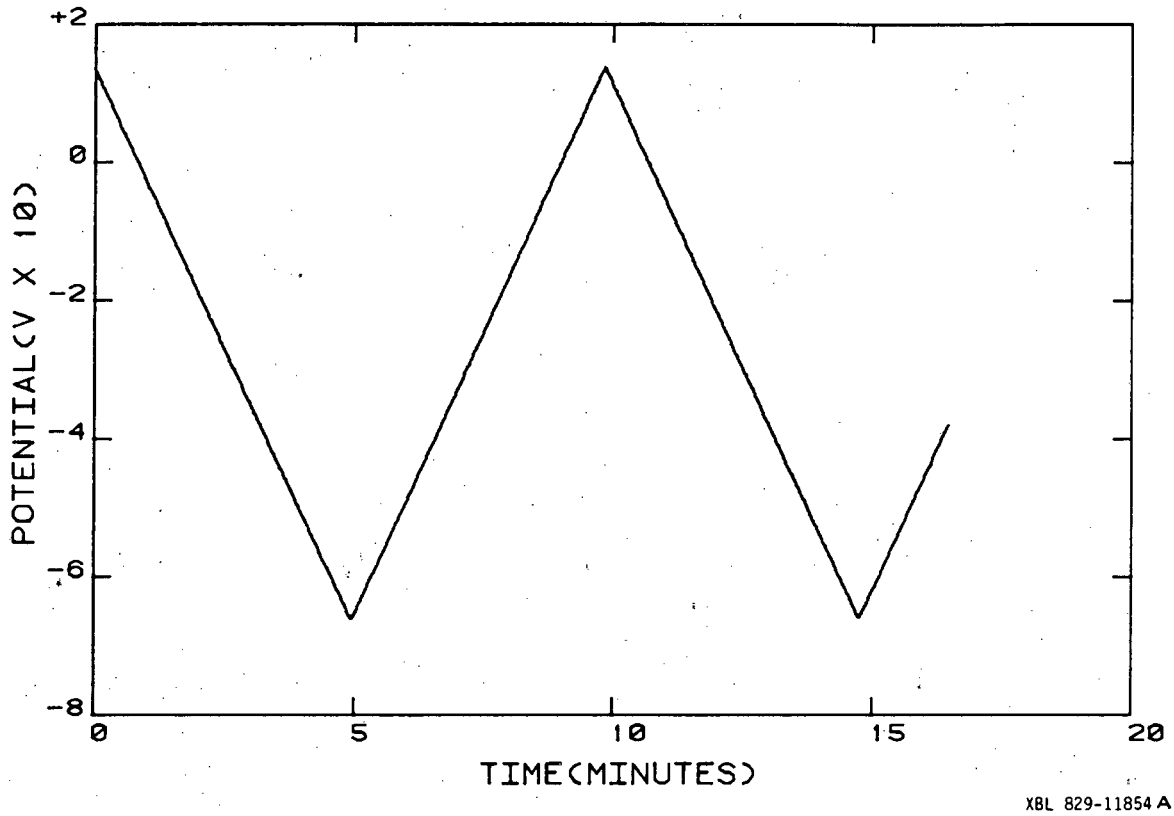
+2
0
-2
-4
-6
-8
POTENTIAL(V X 10)
0
5
10
15
20
TIME(MINUTES)
XBL 829-11854 A

Fig. 2

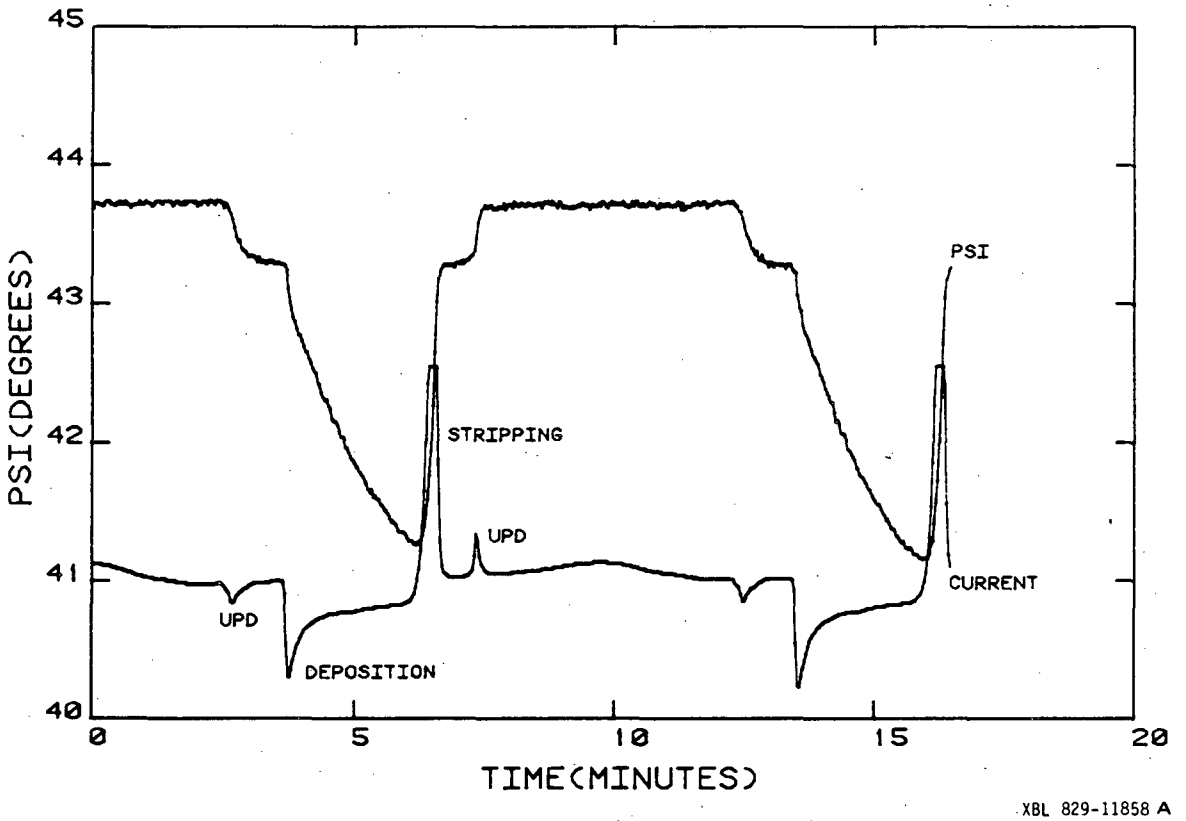
45
44
43
42
41
40
PSI(DEGREES)
0
5
10
15
20
TIME(MINUTES)
PSI
STRIPPING
UPD
UPD
DEPOSITION
CURRENT
XBL 829-11858 A

Fig. 3

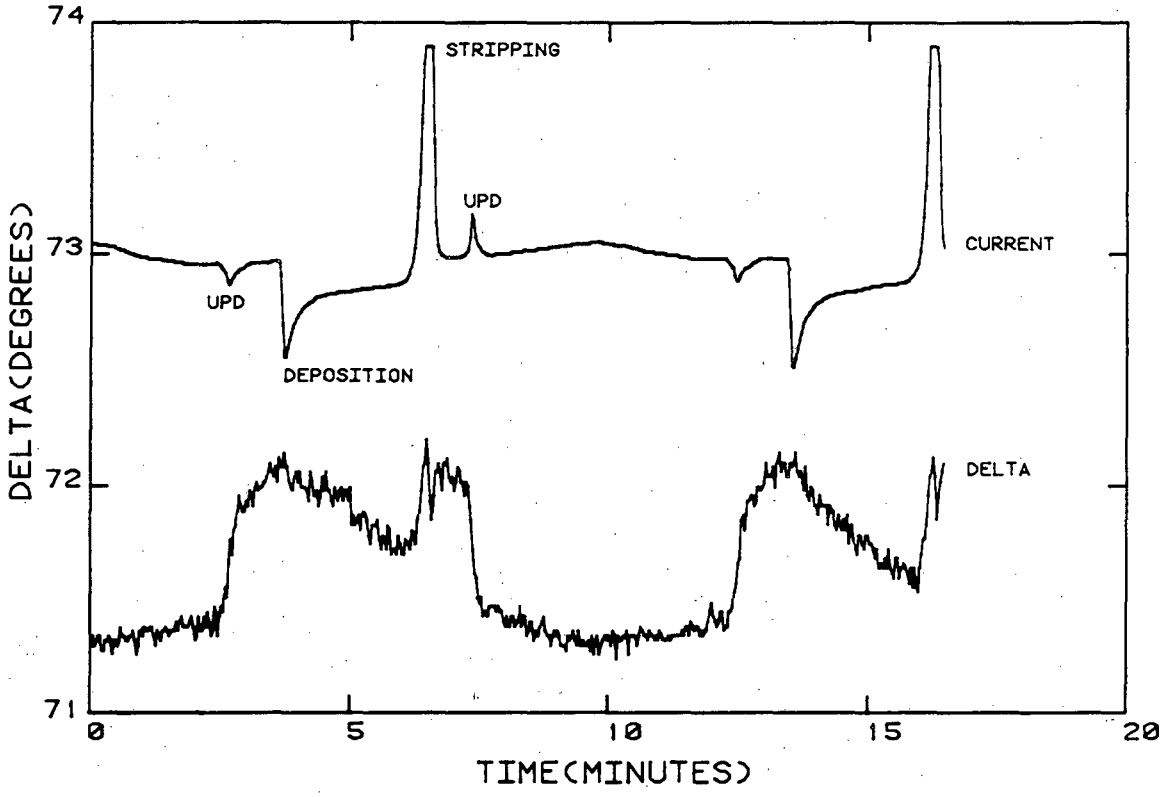

XBL 829-11857B

Fig. 4

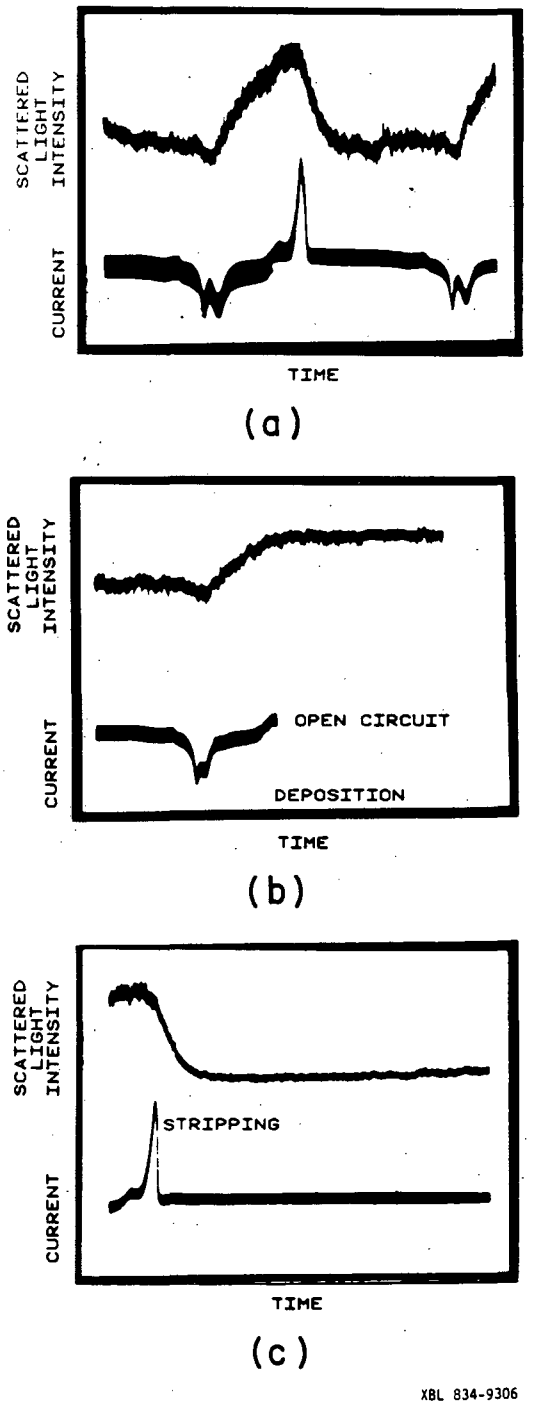
SCATTERED LIGHT INTENSITY
CURRENT
TIME
(a)
SCATTERED LIGHT INTENSITY
CURRENT
OPEN CIRCUIT
DEPOSITION
TIME
(b)
SCATTERED LIGHT INTENSITY
CURRENT
STRIPPING
TIME
(c)
XBL 834-9306

Fig. 5

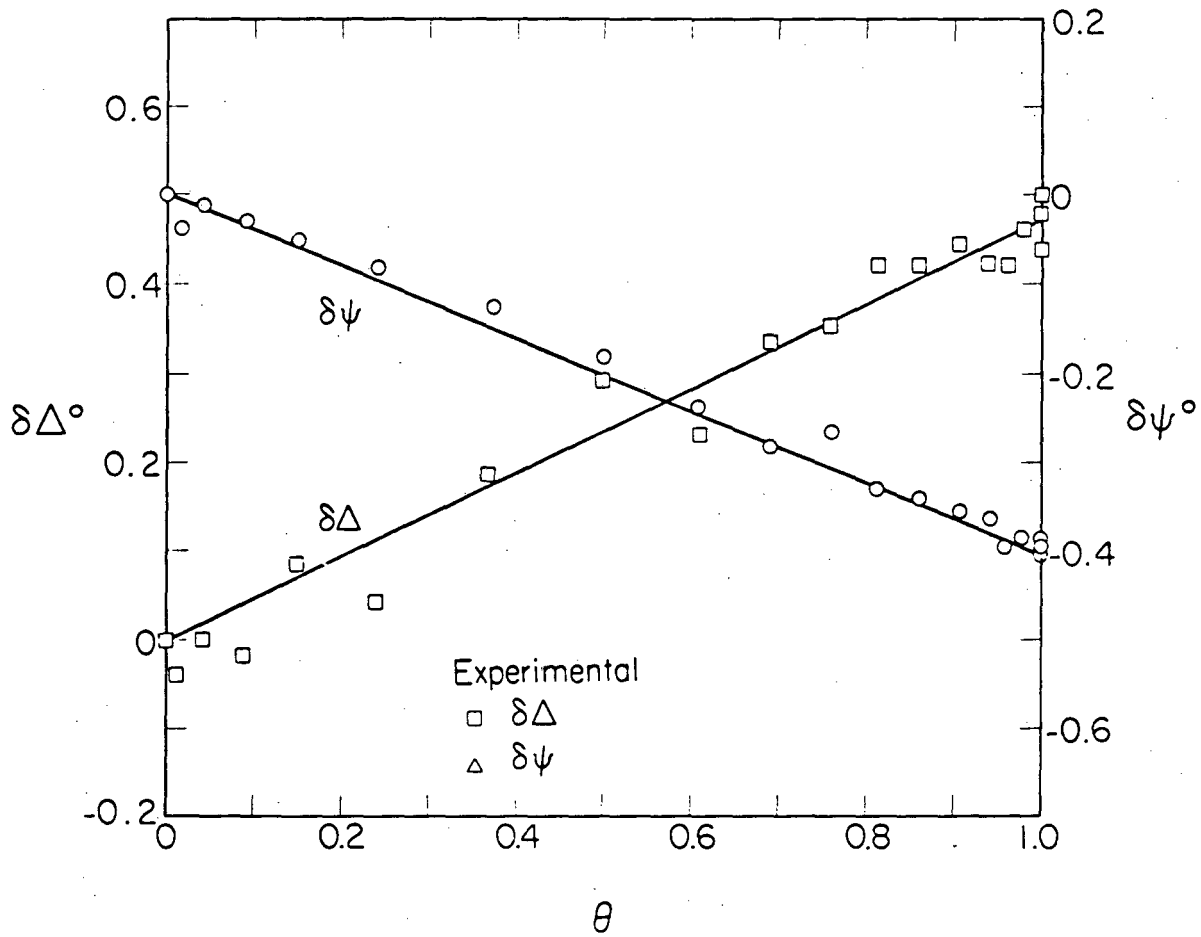

XBL 8212-12373A

Fig. 6

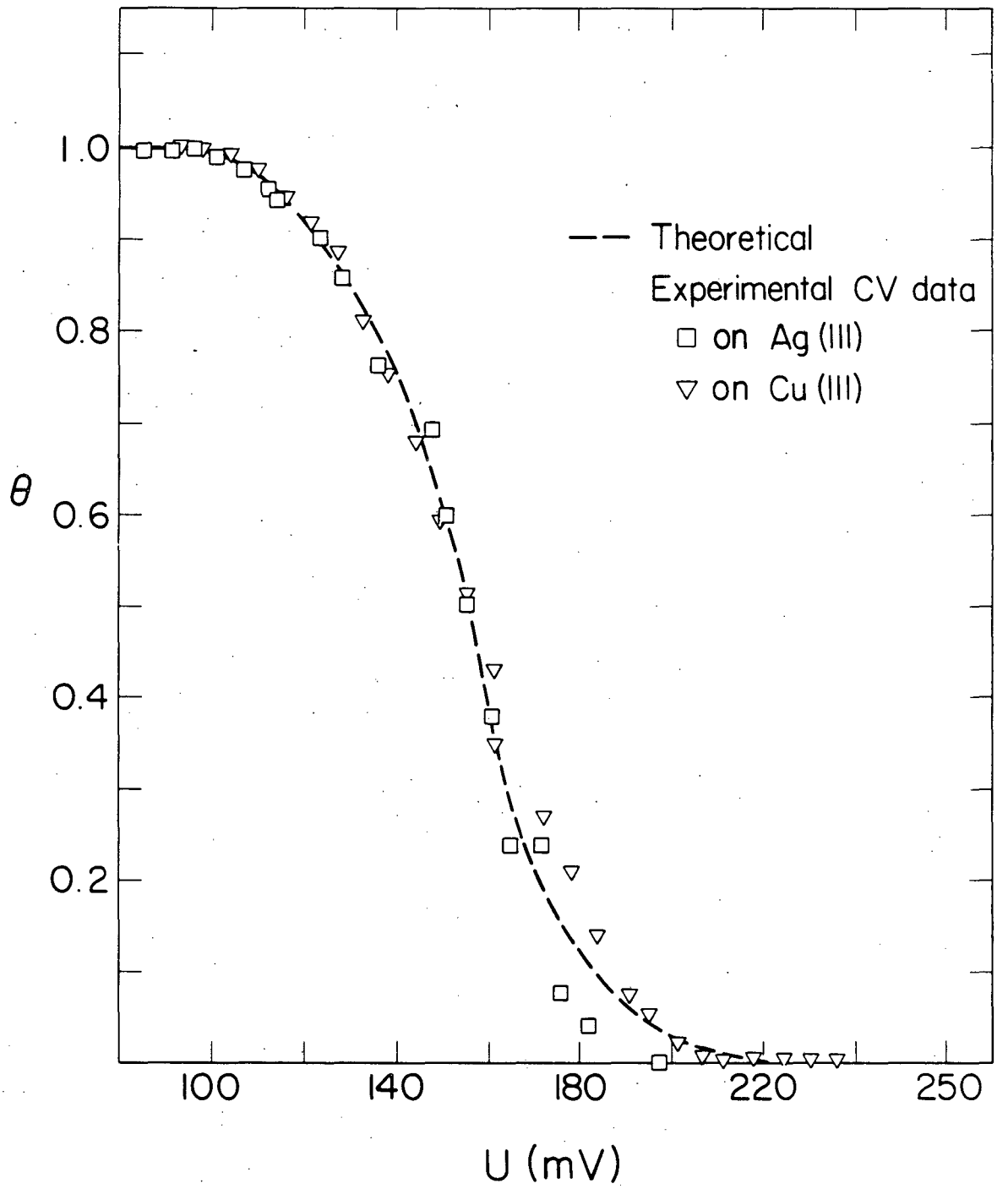

XBL 8212-12372 A

Fig. 7

This report was done with support from the Department of Energy. Any conclusions or opinions expressed in this report represent solely those of the author(s) and not necessarily those of The Regents of the University of California, the Lawrence Berkeley Laboratory or the Department of Energy.

Reference to a company or product name does not imply approval or recommendation of the product by the University of California or the U.S. Department of Energy to the exclusion of others that may be suitable.

TECHNICAL INFORMATION DEPARTMENT
LAWRENCE BERKELEY LABORATORY
UNIVERSITY OF CALIFORNIA
BERKELEY, CALIFORNIA 94720